Available online at www.sciencedirect.com

ScienceDirect

Procedia Computer Science 286 (2026) 48–57

Procedia Computer Science

www.elsevier.com/locate/procedia

Proceedings of the fourth EuroHPC User Days 2026

High-Performance Computing for subsurface flow and transport modelling of Olkiluoto

Albert Costa-Solé[a,*], Emilie Coene[a], Gisela Martí[a], Olga Riba[a], Orlando Silva[a], Tiina Lamminmäki[b], Lasse Koskinen[b], Antti Poteri[b], Antti Joutsen[b], Veli-Matti Pulkkanen[b], Tuomo Karvonen[c], Albin Nordström[d], Guido Deissmann[e]

[a]*Amphos 21 Consulting S.L., C. Pujades 340, 08019 Barcelona, Spain*
[b]*Posiva Oy, FI-27160 Olkiluoto, Eurajoki, Finland*
[c]*Waterhope Oy, FI-00101 Helsinki, Finland*
[d]*Swedish Nuclear Fuel and Waste Management Company (SKB), Solna, Sweden*
[e]*Institute for Energy and Climate Research: Nuclear Waste Management and Reactor Safety (IEK-6) and JARA-HPC, Jülich, Germany*

Abstract

The long-term safety assessment of ONKALO®, the world's first deep geological repository for nuclear waste at Olkiluoto (Finland), requires predicting the hydro-geochemical evolution of a fractured crystalline bedrock over thousands of years. This is done by using a comprehensive/holistic hydro-geochemical reactive transport modelling methodology to add new concepts (e.g., cation exchange, cement leachates) and improve other processes in existing models (e.g., anion exclusion, matrix diffusion, surface hydrology). A significant bottleneck is the Nernst-Planck (NP) formulation used to represent multi-component diffusion processes like anion exclusion. In particular, the NP approach is numerically stiff in large-scale models with approximately 50 million degrees of freedom. This paper presents a cation exchange (CE) formulation equivalent to the NP equations that enables anion exclusion description and reduces significantly the computational cost of large-scale 3D conservative and reactive transport simulations. It also includes an analysis of the scalability of PFLOTRAN on the supercomputer LUMI for production simulations, and the study of the palaeo-hydro-geochemical evolution of the Olkiluoto site using both NP and CE approaches. The results demonstrate that a CE model can be tuned to match the NP formulation, providing a practical tool for further modelling the hydro-geochemical evolution of Olkiluoto.

© 2026 The Authors. Published by Elsevier B.V.
This is an open access article under the CC BY 4.0 license (https://creativecommons.org/licenses/by/4.0)
Peer-review under responsibility of the scientific committee of the Proceedings of the fourth EuroHPC User Days 2026

Keywords: High-Performance Computing; Flow and Transport; PFLOTRAN; Nuclear Waste Repository; Anion Exclusion; Nernst-Planck; Cation Exchange

1. Introduction

Predicting the long-term hydro-geochemical evolution of a deep geological repository for spent nuclear fuel requires solving coupled non-linear equations for flow, multicomponent transport, and geochemistry across a kilometric

* Corresponding author. e-mail: albert.costa@amphos21.com

1877-0509 © 2026 The Authors. Published by Elsevier B.V.
This is an open access article under the CC BY 4.0 license (https://creativecommons.org/licenses/by/4.0)
Peer-review under responsibility of the scientific committee of the Proceedings of the fourth EuroHPC User Days 2026
10.1016/j.procs.2026.08.018

domain over timescales of thousands to a million years. At Olkiluoto on Finland's western coast, these challenges are addressed as Posiva Oy constructs ONKALO®, the world's first final disposal repository [1].

The bedrock is Precambrian crystalline rock (predominantly migmatitic gneisses), with groundwater flow through a complex fracture network characterised by the stochastic ODFN3 Discrete Fracture Network model [2, 3]. The rock matrix (porosity $\varphi_m \approx 0.3$–1%) provides significant solute storage through matrix diffusion, and negatively charged biotite surfaces induce anion exclusion in the matrix pore water, with observed chloride depletion factors of 0.13–0.40 [4, 5]. Groundwater compositions range from fresh meteoric (Cl $\approx$ 3 mg/L) to deep brine (Cl $\approx 42,000$ mg/L) over the time and depth profile [6]. The initial condition of the palaeomodel, 8,100 years ago, consists of a depth-dependent mix of subglacial, saline, and brine waters when the site was fully submerged. The palaeo-evolution includes Littorina seawater infiltration, island emergence (~2,500 years ago) due to post-glacial land uplift (~6 mm/ years), and the development of a meteoric freshwater lens. A sub-horizontal fracture zone (SHF) along the first ~100 m depth strongly controls vertical penetration of surface waters [7].

Numerical simulations are essential for analyzing and demonstrating repository safety. Modeling dissolved sulfide, produced by microbial sulfate reduction, helps predict copper canister corrosion at repository depth (430 m) [8]. Accurately representing fracture-matrix solute exchange and anion exclusion is key, as the coupled evolution of sulfate, iron, hydrogen, and the rock's geochemical buffer all depend on them. The resulting model comprises 3 million cells, 15 transported species, and 50 million degrees of freedom (DOFs), capturing 8,100 years of palaeo-hydro-geochemical evolution with non-linear interactions between density-driven flow and reactive chemistry. High-performance-computing is a key tool to overcome hurdles arising from model complexity coupled with the fabric of the site's hydrogeology.

The OL-STAR project (*OLkiluoto STate-of-Art Reactive hydrogeochemical model*) [9] is a collaboration between Posiva Oy and Amphos 21 Consulting. It was awarded 26.1 million core-hours on the LUMI-C partition under the EuroHPC programme to develop and run PFLOTRAN models [10, 11]. A major computational bottleneck is the representation of anion exclusion in the rock matrix. The Nernst-Planck (NP) equations [12, 4] are physically rigorous but cause severe numerical stiffness; for example, a single 1D case requires about 6 hours, compared to 5 minutes for Fickian transport. To overcome this, it was developed an equivalent cation exchange (CE) formulation that reduces computational cost by ~70× while preserving essential physics. To our knowledge, this work presents for the first time a 3D hydrogeochemical NP-based model addressing anion exclusion at large scale.

2. Modelling framework

The Olkiluoto palaeo-hydro-geochemical model, Fig. 1, couples density-driven groundwater flow with multicomponent reactive transport, solved using PFLOTRAN [10, 11]. The main symbols and notation used throughout the modelling framework are summarised in Table 2.

Saturated groundwater flow follows the mass conservation equation $\frac{\partial(\varphi\rho_w)}{\partial t} + \nabla\cdot(\rho_w\mathbf{q}) = Q_w$, where φ is the porosity, ρ_w the water density, and Q_w a source/sink term. The specific discharge $\mathbf{q}$ is given by Darcy's law with intrinsic tensor permeability $\mathbf{k}$, viscosity μ, and liquid pressure P. Density-dependent flow is driven by the strong salinity gradient and is described using a linear equation of state, $\rho_w = \rho_0 + \beta_s C_s$, where $\rho_0 = 1,000\ \mathrm{kg\,m^{-3}}$ and C_s is the NaCl-equivalent salinity. The coefficient $\beta_s = 40\ \mathrm{g\,mol^{-1}}$ was obtained from a seawater reference density of $\rho_{sw} = 1,024\ \mathrm{kg\,m^{-3}}$ at $C_s = 0.6\ \mathrm{mol\,L^{-1}}$. Transport properties are evaluated at 11 °C, which is the average temperature in the site. Also, pressure effects are neglected, thus focusing on the dominant salinity effect [13].

Transport is solved using PFLOTRAN's Global Implicit Reactive Transport (GIRT) mode. In the fracture continuum, the mass conservation equation for the total concentration Ψ_j^f of each primary species j reads [4, 14]:

$$\frac{\partial(\epsilon_f\varphi_f\Psi_j^f)}{\partial t} + \nabla\cdot(\epsilon_f\mathbf{\Omega}_j^f) = -\epsilon_f\sum_s s\nu_{js}I_s^f - \mathcal{A}_{fm}\mathcal{F}_j^{fm} \tag{1}$$

where ϵ_f is the fracture volume fraction, φ_f the fracture porosity, and $\mathbf{\Omega}_j^f$ is the total flux combining advection, dispersion, and electrochemical contributions. The terms ν_{js} and I_s^f are the stoichiometric coefficient and rate of mineral reaction s, and the last term couples the two continua through the specific interfacial area $\mathcal{A}_{fm}$ (fracture surface area per bulk volume) and the mass exchange flux $\mathcal{F}_j^{fm}$. In the matrix, the same conservation equation applies but without advection ($\mathbf{q} = 0$): transport is purely diffusive, and the modelling approach (Section 2.2 or Section 2.3)

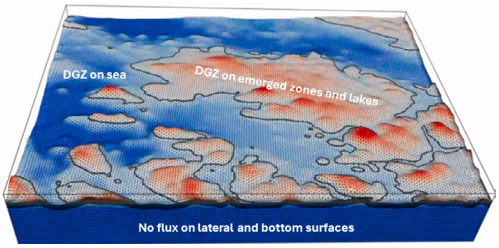


Fig. 1: Computational mesh (2.9 million primary cells) with topography colour-coded by elevation and its associated boundary conditions (DGZ: Dirichlet Zero Gradient). Cutting planes at $y = 2910$ m and $x = 3870$ m reveal bedrock heterogeneity, including fractures, with depth.

determines which diffusion equation is applied: Fickian or Nernst-Planck. Classically, diffusion is represented through Fick's law, which works well when electrochemical effects are not significant. However, in the Olkiluoto system chemical water compositions in the fracture and the rock matrix suggest anion exclusion occurs within the rock matrix. This process is inherently associated with charged mineral surfaces and can be better represented by multicomponent electrochemical diffusion. Nernst-Planck equations are a way of describing the above process [4, 12].

The following subsections describe how these equations are adapted to the dual-continuum representation of the Olkiluoto fractured rock, and how anion exclusion in the matrix is handled.

2.1. The dual-continuum conceptual model

At Olkiluoto, groundwater flows through a network of fractures within a low-permeability rock matrix. The fractures provide pathways for advective transport. The matrix, by contrast, acts as an immobile storage reservoir accessible only by diffusion. This creates a natural separation of timescales: solutes move rapidly through fractures but exchange slowly with the surrounding rock over distances of centimetres to meters. This exchange controls the long-term evolution of groundwater chemistry and sulfide concentrations at repository depth.

This physical picture is represented using a Dual Continuum Disconnected Matrix Model (DCDMM) and an Equivalent Continuum Porous Media (ECPM) approach [14, 15], in which the rock volume is partitioned into two overlapping continua. The primary (fracture) continuum carries advective and dispersive transport through a 3D mesh of 2.9 million cells (Fig. 1), with heterogeneous properties upscaled from the ODFN3 Discrete Fracture Network model [2] (Fig. 2). Fig. 2 illustrates two upscaled ECPM fields used by the dual-continuum model. The left panel shows the intrinsic permeability in the x direction, whereas the right panel shows the matrix half-length derived from the local DFN fracture statistics.

During the Olkiluoto island emergence, the top surface boundary conditions are split into three zones (Fig. 1): sea (Dirichlet with evolving Littorina-to-Baltic sea chemical composition and atmospheric pressure at the sea level), emerged land (Dirichlet with meteoric water composition and prescribed recharge), and lakes (Dirichlet with meteoric water composition and prescribed head). Lateral and bottom boundaries are set as no-flux for flow and transport. Time-dependent boundary conditions (shoreline displacement, evolving seawater composition, and heterogeneous effective recharge) are managed using an in-house Python script that updates these parameters at each time step.

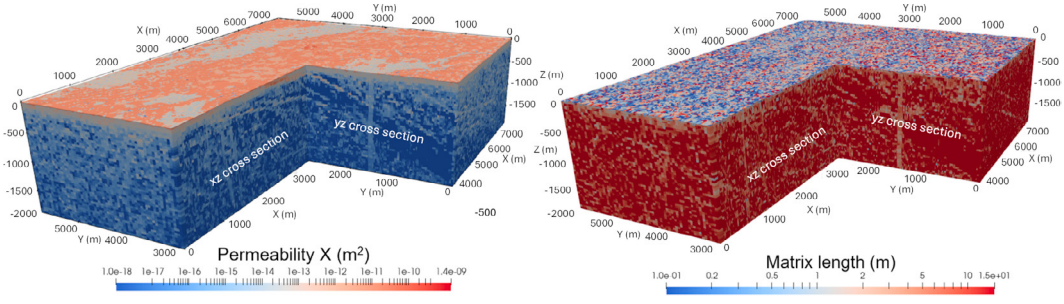


Fig. 2: ECPM properties upscaled from the ODFN3 Discrete Fracture Network model. Left: intrinsic permeability in the x-direction. Right: matrix half-length. Both fields are heterogeneous and reflect the local DFN fracture statistics.

Each fracture cell (primary continuum) is connected to a 1D line of 10 matrix cells (secondary continuum), through which solutes diffuse perpendicular to the fracture wall. In the matrix, advection is absent, and the mass balance equation for species j reduces to [14]:

$$\frac{\partial(\varphi_m \Psi_j^m)}{\partial t} + \nabla_\xi \cdot \mathbf{\Omega}_j^m = -\sum_s s\nu_{js} I_s^m \tag{2}$$

where ∇_ξ is the gradient operator in the secondary continuum coordinate ξ (distance from the fracture-matrix interface) and $\mathbf{\Omega}_j^m$ is the matrix diffusive flux, with species-dependent effective diffusion coefficient combining the matrix tortuosity and the species self-diffusion coefficient [4]. In the standard Fickian model, all species share a single diffusion coefficient; when electromigration is considered (Section 2.2), $\mathbf{\Omega}_j^m$ includes an additional electrochemical term. The fracture-matrix coupling in Eq. (1) is computed from the flux at the outer boundary of the matrix continuum (fracture-matrix interface) as $\mathcal{F}_j^{fm} = \mathbf{\Omega} j^m \cdot \mathbf{n}\big|\xi = \xi_{\text{out}}$ [4, 14]. This expression represents the continuity of total concentration at the fracture-matrix interface. In addition, zero-flux is assumed at the innermost cell in the matrix [14]. The matrix is characterised by its porosity φ_m and half-length L_m. The L_m is derived from the local DFN statistics and varying across the domain. Geochemical reactions (mineral dissolution, cation exchange, and microbial processes) occur independently in both continua. Salinity is tracked through an auxiliary tracer defined as a weighted sum of Cl^-, Na^+, Ca^{2+}, and Br^-.

2.2. Anion exclusion: the Nernst-Planck formulation

In the standard Fickian model, the matrix diffusive flux $\mathbf{\Omega}_j^m$ in Eq. (2) uses a single effective diffusion coefficient D_m for all species. However, the negatively charged surfaces of biotite and other clay minerals in the Olkiluoto matrix create a permanent electrical field that repels anions and attracts cations, reducing the effective porosity available for anion transport. In the NP formulation [4, 12], this effect is modelled by representing the mineral surface charge as a fixed concentration of immobile anions Q (eq/L). The presence of Q establishes a Donnan potential ψ_D that partitions ions between the charged and bulk porosity:

$$\xi_i = C_i^D / C_i^B = \Gamma_i \exp\left(-z_i F \psi_D / RT\right) \tag{3}$$

where z_i is the ion charge, F the Faraday constant, R the gas constant, T the absolute temperature, and the superscripts D and B denote the Donnan and bulk porosity, respectively. Because the exponential depends on z_i, divalent sulfate ($z = -2$) is excluded more strongly than monovalent chloride ($z = -1$) for the same ψ_D.

The Nernst-Planck equation replaces the Fickian flux for each individual species i with a coupled electrochemical flux [4]:

$$\mathbf{J} i^m = -\varphi_m D_i^m \left(\nabla \xi c_i - z_i c_i \frac{\sum_j D_j^m z_j \nabla_\xi c_j}{\sum_k z_k^2 D_k^m c_k} \right) \tag{4}$$

where D_i^m is the species-dependent pore diffusion coefficient in the matrix (product of matrix tortuosity and self-diffusion coefficient in unconstrained solution). The first term is Fickian diffusion; the second couples all charged species through an electromigration term that enforces electroneutrality. Physically, when a fast-diffusing ion such as Cl^- moves ahead of a slower counter-ion such as Ca^{2+}, an electrical potential builds up that retards the faster ion and accelerates the slower one. Numerical evaluation requires logarithmic averaging at cell interfaces [16] to avoid artefacts for asymmetric electrolytes. The resulting system is stiff, due to a 1D case of a fracture at 200 m depth requires approximately 6 hours, compared to 5 minutes for the equivalent Fickian model, making the direct application of NP in 3D reactive transport impractical without supercomputing.

2.3. The cation exchange formulation

To make anion exclusion computationally tractable at the site scale, it was developed a CE formulation that reproduces the macroscopic effect of the NP equations without replacing the Fickian flux. Instead, it modifies the storage terms in the matrix transport equation (Eq. (2)).

The central parameter is the anion-accessible porosity fraction, $f_a = \sum_i c_i^m |z_i| / \sum_i c_i^f |z_i|$ (5), defined as the ratio of charge-weighted anion concentrations in the matrix (c_i^m) to those in the fracture (c_i^f), with z_i the ion charge. This definition follows directly from the Donnan equilibrium (Eq. (3)): the partitioning of each anion depends on the Donnan potential, and the charge-weighted average yields an effective macroscopic f_a. Because the Donnan potential

Table 1: Scalability on Jureca [17] and LUMI. DOFs is DOFs per task. Bold: production.

Nodes	Tasks	LUMI	JURECA	DOFs	Efficiency
4 nodes	512	✓	✓	97 656	1.00
8 nodes	1 024	✓	✓	48 828	0.94
16 nodes	2 048	✓	✓	24 414	0.79
32 nodes	**4 096**	✓	×	**12 207**	**0.65**
64 nodes	8 192	✓	×	6 104	0.42
256 nodes	16 384	✓	×	3 052	0.22

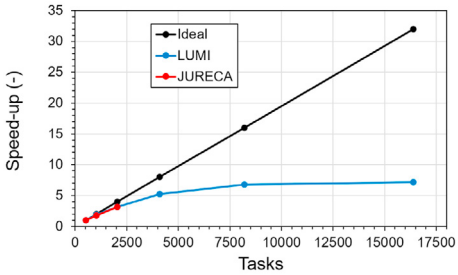


Fig. 3: Scalability for the palaeo-evolution (~50 M DOFs).

depends on the ionic strength relative to the fixed charge Q, f_a is not a material constant but varies with the local salinity: at high ionic strengths, anion exclusion is weak and f_a approaches unity; in dilute waters, f_a decreases substantially.

Using f_a, the matrix porosity is partitioned into an anion-accessible volume and a complementary volume where cations are retained on exchange sites that compensate the mineral surface charge. The overall matrix concentration of an anion is $c_i^m = f_a \bar{c}_i^m$, being $\bar{c}_i^m$ the concentration in the anion accessible porosity. For an exchangeable cation, it includes the exchanger contribution as $c_i^m = f_a \bar{c}_i^m + \mathrm{CEC} \cdot N_i$, where CEC is the cation exchange capacity and N_i is the equivalent fraction on the exchange sites.

The equivalence between the CE and NP approaches has been established through the f_a parameter, which has been estimated with the NP-predicted anion distribution ratio (Eq. (3)). A known limitation is that f_a is charge-independent: unlike NP, which predicts stronger exclusion for divalent anions, the CE approach applies the same accessible fraction to all anions. Despite this simplification, the CE approach captures the dominant effect: the overall reduction in anion mass transfer between fractures and the matrix, which is the primary control on the chloride and sulfate profiles used for model calibration. A 1D proxy model confirmed that CE and NP produce practically identical chloride profiles, while full NP predicts somewhat stronger divalent exclusion. The 1D CE model runs in approximately 5 minutes, compared with approximately 6 hours for NP, resulting in a roughly 70-fold cost reduction.

3. HPC deployment on LUMI

The Olkiluoto palaeomodel (2.9 million primary cells with 10 secondary continuum cells each, 15 chemical species plus flow, yielding ~50 million DOFs) was deployed on the LUMI-C partition, compiled with the Cray compiler environment, PETSc 3.21.5, and parallel HDF5 for I/O. Using fewer than 128 cores (1 node) is impractical for models of this size: each MPI task requires at least 500 MB of RAM for the secondary continuum arrays alone, and wall-clock times on a single node would extend to weeks.

The model was tested from 512 to 16,384 MPI tasks (Table 1, Fig. 3) by simulating the submerged period of the palaeo-evolution of Olkiluoto using a semi-structured mesh, which includes matrix diffusion and reaction. We observe that scalability is governed by the ratio of DOFs per MPI process: above ~10,000 DOFs/task, the computation is dominated by local linear algebra and secondary continuum solves, both of which scale well; below this threshold, inter-process communication begins to dominate. The practical optimum was found at 4,096 tasks across 32 nodes (128 tasks/node), where the measured speed-up relative to 512 tasks is approximately 5.2, corresponding to a strong-scaling efficiency of about 65% because the number of tasks increases by a factor of eight. This configuration was adopted for all production runs. Beyond 4,096 tasks, performance degrades as DOFs/task drop to ~6,000 (8,192 tasks) and ~3,000 (16,384 tasks), at which point the communication-to-computation ratio becomes unfavourable. For comparison, the same model was tested on JURECA-DC up to 2,048 tasks with consistent results; higher configurations could not be tested in JURECA due to PETSc segmentation faults traced to library version incompatibilities, which underscores the importance of cross-platform verification for production HPC codes. At the production configuration, a single 8,100-year palaeo-hydro-geochemical simulation completes in 24–48 wall-clock hours, consuming 100,000–200,000 core-hours depending on the complexity of the reactive system. Time-to-solution is problem-dependent: conservative transport with Fick's diffusion is the fastest, the CE formulation is intermediate, and nonlinear diffusion represented by NP equations is the most expensive due to the stiffness introduced by the electromigration terms. The numerical solution relies on PETSc-based solvers. Both the flow and transport systems use Newton's method, with FGMRES and Additive Schwarz preconditioning for the transport linear system and standard GMRES for the flow system. Sep-

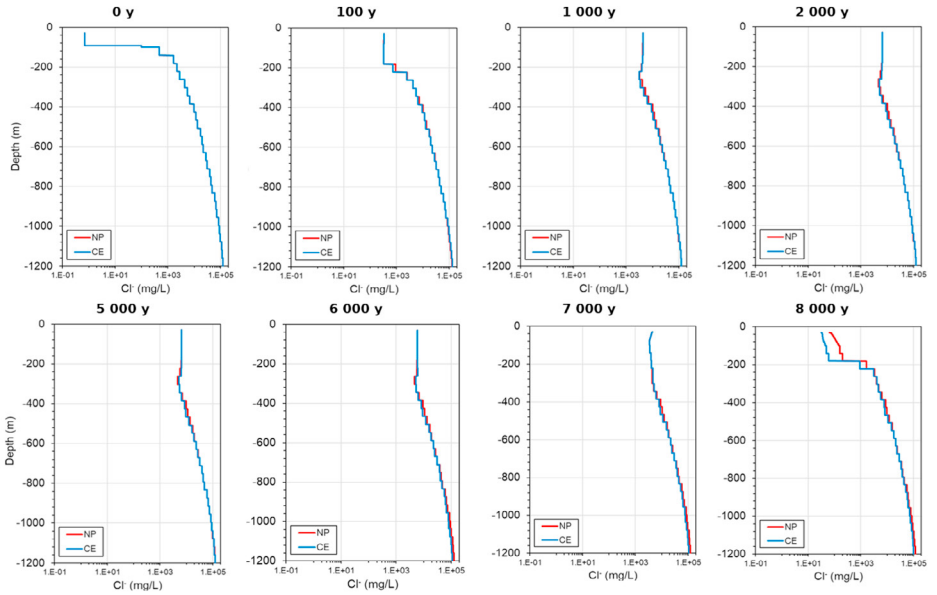


Fig. 4: Temporal evolution of chloride concentration vertical profiles. Blue: CE (f_a = 0.167); red: NP. CE parameterisation: NP with Q = 0.1 M. CE parametrization with CEC = 2.1 mol/m^3,$\phi_m = 6.3 \times 10^{-3}$.

arate convergence tolerances are enforced for the primary and secondary continuum unknowns to prevent the matrix diffusion equations from stalling global convergence. An adaptive time stepper with aggressive acceleration allows large steps during quasi-steady phases while retreating automatically during sharp transients. A complete modelling campaign (several ECPM realisations, multiple f_a sensitivity runs, and NP vs. CE comparisons) demands several million core-hours, well beyond institutional cluster capacity and justifying the EuroHPC allocation.

4. Results and discussion

This section presents the main results of the OL-STAR palaeo-hydro-geochemical conservative transport simulations in three parts. First, the equivalence between the NP and CE formulations is validated through temporal chloride profiles and a multispecies comparison at 8,100 y (Section 4.1). Second, the sensitivity of model predictions to the anion-accessible fraction f_a is evaluated against monitoring borehole data, and the robustness of the results with respect to matrix discretisation is demonstrated (Section 4.2). Third, the 3D chloride and sulfate distribution at 8,100 years is presented as vertical cross-sections through the model domain (Section 4.3).

4.1. NP–CE equivalence: temporal evolution and multispecies validation

A prerequisite for using the CE formulation in production 3D simulations is to confirm that it reproduces the NP solution across the full range of hydrogeochemical conditions encountered during the palaeo-evolution. Fig. 4 compares vertical chloride concentration profiles at the centre of the 3D domain shown in from the NP and CE (f_a = 0.167, CEC = 2.1 mol/m^3, Q = 0.1 M, $\phi_m = 6.3 \times 10^{-3}$) models at eight time snapshots. During the submerged phase, Littorina seawater progressively displaces subglacial water in the upper 400 m, while concentrations below 400 m reach quasi-steady state. After the island emergence (~7,100 years), meteoric infiltration creates a freshwater lens in the bedrock above 100–200 m depth. Throughout this evolution, the NP and CE profiles overlap almost perfectly. Divergence appears only in the latest stages (7,000–8,100 years) within the upper 200 m, where the freshwater lens produces low-salinity conditions that amplify the difference between charge-dependent NP partitioning and the CE model with constant f_a. Physically, dilution in the shallow zone reduces the ionic strength causing the NP formulation to predict a stronger Donnan exclusion than the constant f_a assumed by the CE model. As a result, the CE model allows slightly more freshwater penetration into the matrix. This behaviour is consistent with the theoretical expectation that the CE simplification becomes less accurate as salinity decreases relative to the fixed charge.

The multispecies comparison at 8 100 years (Fig. 5) extends the validation beyond chloride to all 10 transported species. The equivalent CE model was run for two values of f_a: 0.167 and 0.53. With f_a = 0.53, the CE model

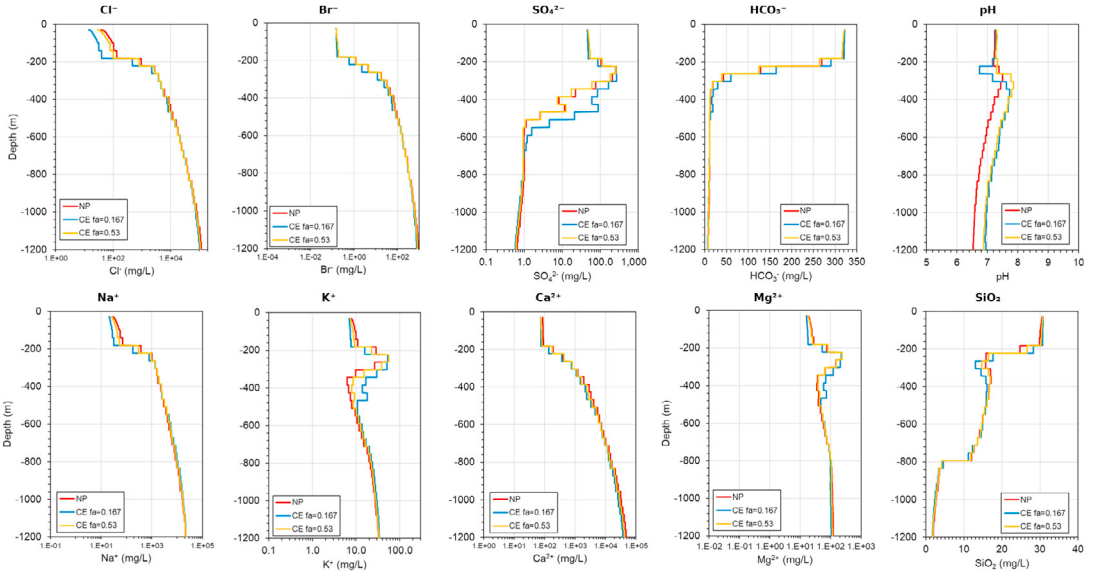


Fig. 5: 1D vertical concentration profiles of 10 species at 8,100 y: NP (red) vs. CE with $f_a = 0.167$ (blue) and $f_a = 0.53$ (yellow). CE parameterisation: CEC = 2.1 mol/m^3, $\phi_m = 6.3 \times 10^{-3}$.

closely reproduces the NP depth profiles for the monovalent anions Cl^- and Br^-, and provides a reasonable match for Na^+, K^+, Ca^{2+}, and SiO_2. The largest deviations appear for SO_4^{2-} in the Subglacial-Saline zone (200–600 m), where the charge-independent f_a of the CE formulation cannot reproduce the stronger divalent exclusion predicted by NP (Eq. (3)). Mg^{2+} and HCO_3^- also show notable differences in the upper 400 m, while pH is sensitive to the choice of f_a only locally, and both CE simulations produce different results than NP. Using $f_a = 0.167$ generally shifts all CE profiles further from the NP reference, most visibly for the anions in the shallow zone where anion exclusion is strongest. This illustrates that the choice of f_a has a quantifiable impact on predicted concentrations and must be treated as a calibration target if a comparison with NP is performed.

The combination of the CE formulation and High-Performance-Computing resources is the key enabling factor demonstrated here. Before this work, the NP approach was limited to 1D case models requiring hours per run; the CE approach reduces the per-simulation cost by ~70×, to the point where LUMI can deliver production 3D runs in 24–48 h and support systematic sensitivity analysis across the multi-dimensional parameter space (φ_m, f_a, Q).

4.2. Sensitivity to f_a, comparison with field data, and matrix discretisation

The anion accessible porosity fraction f_a (Eq. (5)) is the central calibration parameter of the CE formulation. As discussed in Section 2.3, f_a is not an intrinsic material parameter but depends on the local salinity through the Donnan potential. The NP-derived values in our simulations range from 0.41 near the surface (where meteoric dilution is strongest) to 0.90 at depth (where brine salinities dominate). This depth dependence is the fundamental reason why a single constant f_a cannot perfectly reproduce the NP solution at all depths, and why f_a must be calibrated against field data. The ability to quantify this effect through systematic 3D sensitivity analysis represents a practical advance for the safety case.

Fig. 6 shows the f_a sensitivity at 8,100 years for chloride, compared against monitoring borehole data. Chloride (top row), as a monovalent anion, is sensitive to f_a primarily in the upper 400 m, where the contrast between the dilute meteoric lens and the deeper saline waters amplifies the effect of anion exclusion on matrix–fracture exchange. It can be observed that f_a does not impact the concentration fields significantly. In general, the model shows high infiltration of meteoric water. This effect is mitigated for higher fractions of anion accessible porosity. The effect is mainly visible at low f_a values, beyond $f_a = 0.4$ results are comparable. The regions with higher concentrations correspond to submerged areas, where there is no recharge. Because the fracture–matrix solute exchange in the DCDMM depends on the size of the cell adjacent to the fracture-matrix interface, we tested the sensitivity of the results to the number of matrix cells (Fig. 7). Three configurations were compared: 5 cells (coarse mesh), 10 cells (base case), and 20 cells (fine mesh), all using $f_a = 0.9$ and the same CE parameterisation ($Q = 0.1$ M, $f_m = 6.3 \times 10^{-3}$). The depth profiles

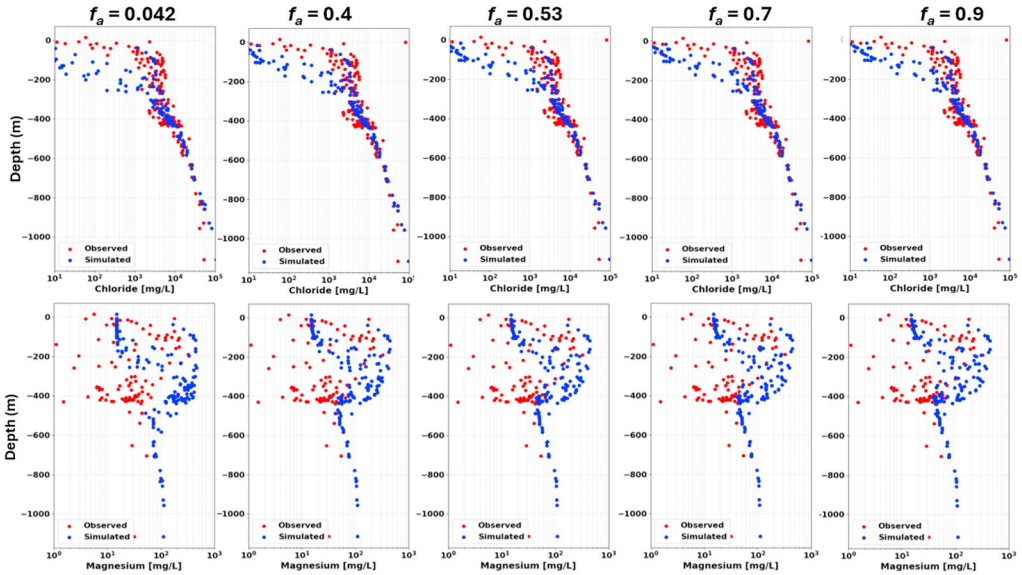


Fig. 6: Sensitivity of the model to anion accessible porosity fraction. Vertical concentration profiles of chloride (top) and magnesium (bottom) at 8, 100 years. Red: observed borehole data; blue: simulated.

of all 10 species are essentially insensitive to the matrix discretisation, with minor differences confined to the vicinity of sharp transport fronts. This confirms that the base-case discretisation of 10 matrix cells adequately resolves the diffusion gradients and that the model results are numerically robust.

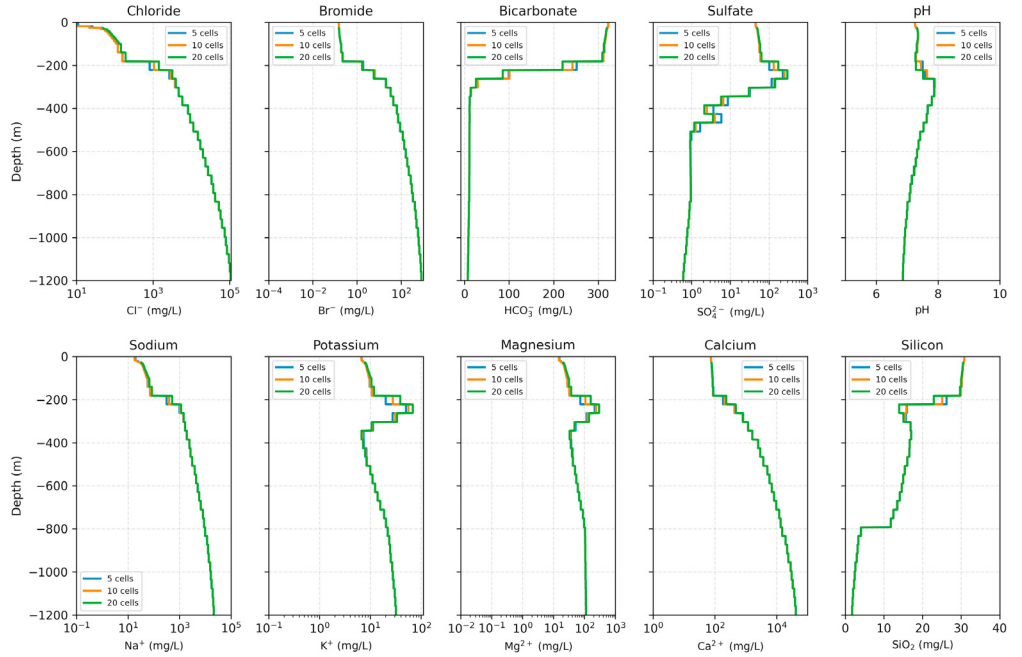


Fig. 7: Sensitivity of the model to the spatial matrix length discretisation (5, 10 and 20 cells). Concentration profiles at 8, 100 years.

4.3. 3D chloride distribution at 8,100 years

Chloride and sulfate are key species controlling density-driven flow and sulfide formation, respectively. The spatial distributions of these species at 8,100 years are shown in Fig. 8 as vertical cross-sections through the 3D CE model

domain. The xz section (at $y = 2,910$ m) and yz section (at $x = 3,870$ m) show the expected hydrogeochemical palaeo-evolution at Olkiluoto: a shallow freshwater lens (Cl $<$ 100 mg/L) resulting from post-emergence meteoric infiltration, a brackish Littorina-derived zone at intermediate depth (100–400 m), and deep saline-to-brine waters (Cl $>$ 10,000 mg/L) that have remained largely undisturbed since before 8,100 years. The freshwater penetration is deepest beneath topographic elevations and above the sub-horizontal fracture zone at ~140 m, consistent with the enhanced horizontal connectivity in this zone. These cross-sections demonstrate that the CE model, calibrated against depth profiles and monitoring data, reproduces the expected large-scale solute architecture at the full 3D site scale.

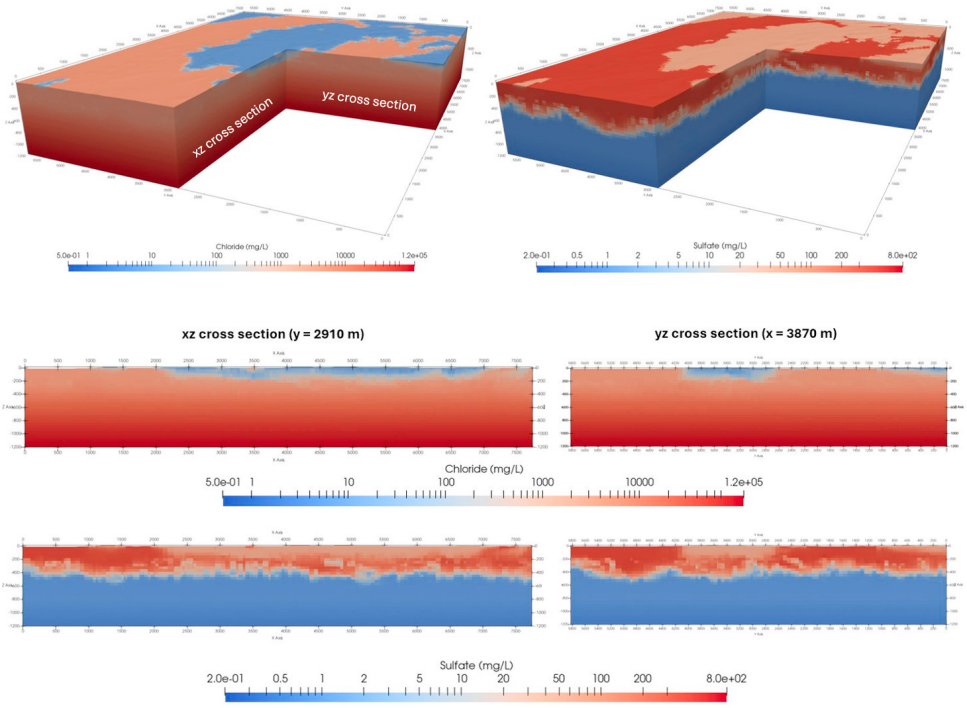


Fig. 8: Chloride and sulfate concentration distributions at 8,100 y through the CE model ($f_a = 0.9$).

5. Conclusions

This work demonstrates that the combination of a cation exchange modelling approach (CE) for anion exclusion and supercomputing resources enables 3D site-scale conservative and reactive transport modelling that was previously unfeasible for nuclear waste safety assessment. The approach was applied to simulate the hydrogeochemical palaeo-evolution of Olkiluoto site selected to build the first deep nuclear waste storage repository of the world.

The CE formulation, validated here against the full Nernst-Planck (NP) equations in both temporal and multispecies 3D configurations, reduces drastically the computational cost while preserving the essential physics. The NP-derived anion accessible porosity fraction f_a (Eq. (5)) provides a calibration target that links the CE parametrization to the underlying Donnan partitioning mechanism. All the presented results were mainly computed using the LUMI-C partition with 4,096 MPI tasks (approximately 65% strong-scaling efficiency relative to 512 tasks, and approximately 50 million degrees of freedom). Each 8,100-year palaeo-hydro-geochemical simulation completes in 24–48 wall-clock hours. This performance makes systematic sensitivity analysis and multi-realisation studies operationally viable. The simulations reproduce the observed groundwater stratification at Olkiluoto, including the freshwater lens, comparable to the spatial variability in the monitoring data.

These results establish a validated modelling foundation for the next phase of the OL-STAR project, which will focus on three objectives: (i) automated calibration across several ECPM stochastic realisations using the Optuna optimisation framework; (ii) integration of chemical reactions including microbially mediated sulfide production into the 3D reactive transport framework; and (iii) long-term post-closure simulations under future climate scenarios.

Code and data availability

The availability of datasets is subject to project confidentiality. PFLOTRAN is an open source code.

Nomenclature

Table 2: Nomenclature used in the governing equations.

Symbol	Meaning	Units	Symbol	Meaning	Units
$\varphi, \varphi_f, \varphi_m$	Total, fracture and matrix porosity	–	$\mathcal{F}_j^{fm}$	Fracture–matrix exchange flux	$\mathrm{mol\,m^{-2}\,s^{-1}}$
ρ_w, ρ_0	Water density and reference density	$\mathrm{kg\,m^{-3}}$	ξ	Matrix-continuum coordinate	m
$\mathbf{q}$	Darcy specific discharge	$\mathrm{m\,s^{-1}}$	L_m	Matrix half-length	m
Q_w	Water source/sink term	$\mathrm{kg\,m^{-3}\,s^{-1}}$	D_i^m	Matrix pore diffusion coefficient	$\mathrm{m^2\,s^{-1}}$
$\mathbf{k}$	Intrinsic permeability tensor	$\mathrm{m^2}$	z_i	Ionic charge of species i	–
μ	Dynamic viscosity	Pa s	F	Faraday constant	$\mathrm{C\,mol^{-1}}$
P	Liquid pressure	Pa	R	Gas constant	$\mathrm{J\,mol^{-1}\,K^{-1}}$
Ψ_j	Total concentration of species j	$\mathrm{mol\,m^{-3}}$	T	Absolute temperature	K
$\mathbf{\Omega}_j$	Total solute flux of species j	$\mathrm{mol\,m^{-2}\,s^{-1}}$	ψ_D	Donnan potential	V
ϵ_f	Fracture volume fraction	–	Q	Fixed immobile charge concentration	$\mathrm{eq\,L^{-1}}$
ν_{js}	Stoichiometric coefficient	–	f_a	Anion-accessible porosity fraction	–
I_s	Mineral reaction rate	$\mathrm{mol\,m^{-3}\,s^{-1}}$	CEC	Cation exchange capacity	$\mathrm{mol\,m^{-3}}$
$\mathcal{A}_{fm}$	Fracture–matrix interfacial area	$\mathrm{m^{-1}}$	N_i	Equivalent fraction on exchange sites	–

Acknowledgements

We acknowledge EuroHPC JU for awarding the project ID EHPC-REG-2025R02-204 and EHPC-REG-2022R03-225 access to the LUMI-C partition hosted by CSC – IT Center for Science Ltd. (Finland). The authors gratefully acknowledge computing time on the supercomputer JURECA at Forschungszentrum Jülich (Germany) under grant no. JIEK63. The OL-STAR project is funded by Posiva Oy.

References

[1] Posiva Oy, Olkiluoto Site Description 2018, Technical Report POSIVA 2021-10, Posiva Oy, Eurajoki, Finland, 2021.
[2] L. Hartley, P. Appleyard, S. Baxter, J. Hoek, D. Roberts, D. Swan, Hydrogeological structure model of Olkiluoto, Technical Report Posiva WR 2018-32, Posiva Oy, Eurajoki, Finland, 2018.
[3] P. Aalto, et al., Hydrogeology of Olkiluoto, Technical Report POSIVA 2021-15, Posiva Oy, Eurajoki, Finland, 2021.
[4] P. Trinchero, A. Nardi, O. Silva, P. Bruch, Simulating electrochemical migration and anion exclusion in porous and fractured media using pflotrannp, Computers & Geosciences 166 (2022) 105166.
[5] F. Eichinger, et al., Matrix pore water at Olkiluoto, Technical Report Posiva 2006-103, Posiva Oy, Eurajoki, Finland, 2006.
[6] Posiva Oy, Palaeohydrogeochemical Data for Olkiluoto, Technical Report POSIVA 2021-13, Posiva Oy, Eurajoki, Finland, 2021.
[7] T. Karvonen, Surface hydrology model of Olkiluoto, Working Report, Posiva Oy, Eurajoki, Finland, 2021.
[8] Posiva Oy, Sulfide Fluxes at Olkiluoto – 2021 Update, Technical Report POSIVA WR 2021-07, Posiva Oy, Eurajoki, Finland, 2021.
[9] Posiva Oy, Amphos 21 Consulting, OL-STAR: EuroHPC JU Final Report, Technical Report EHPC-REG-2022R03-225, EuroHPC Joint Undertaking, 2025.
[10] P. C. Lichtner, G. E. Hammond, C. Lu, S. Karra, G. Bisht, B. Andre, R. Mills, J. Kumar, PFLOTRAN user manual: A massively parallel reactive flow and transport model for describing surface and subsurface processes, Technical Report, Los Alamos National Lab.(LANL), Los Alamos, NM (United States); Sandia . . . , 2015.
[11] G. E. Hammond, P. C. Lichtner, R. Mills, Evaluating the performance of parallel subsurface simulators: An illustrative example with pflotran, Water resources research 50 (2014) 208–228.
[12] T. Gimmi, P. Alt-Epping, Simulating donnan equilibria based on the nernst-planck equation, Geochimica et Cosmochimica Acta 232 (2018) 1–13.
[13] IOC, SCOR and IAPSO, The international thermodynamic equation of seawater – 2010: Calculation and use of thermodynamic properties, Intergovernmental Oceanographic Commission, UNESCO, 2010.
[14] A. Iraola, P. Trinchero, S. Karra, J. Molinero, Assessing dual continuum method for multicomponent reactive transport, Computers & Geosciences 130 (2019) 11–19.
[15] P. C. Lichtner, S. Karra, Modeling multiscale-multiphase-multicomponent reactive flows in porous media: Application to co2 sequestration and enhanced geothermal energy using pflotran, Computational Models for CO2 Geo-sequestration & Compressed Air Energy Storage (2014) 81–136.
[16] C. Tournassat, C. I. Steefel, T. Gimmi, Solving the nernst-planck equation in heterogeneous porous media with finite volume methods: Averaging approaches at interfaces, Water resources research 56 (2020) e2019WR026832.
[17] P. Thörnig, JURECA: Data-centric and booster modules implementing the modular supercomputing architecture at Jülich supercomputing centre, Journal of Large-Scale Research Facilities 7 (2021) A182–A182.